I.A.U
Karaj branch

Journal of
A p p l ied
C hemical
R esearch
jacr.kiau.ac.ir

Journal of Applied Chemical Research, 17, 4, 8-21 (2023)

Investigation of the Structural and Electrical Properties of Star Shape Manganese Thin Films with 3-fold and 4-fold Symmetries

Fatemeh Abdi

Department of Engineering Sciences, Faculty of Advanced Technologies, University of Mohaghegh Ardabili, Namin, Iran

(Received 21 Feb. 2023; Final revised received 14 May 2023)

Abstract

Manganese star shape sculptured thin films with 3-fold and 4-fold symmetries were formed on glass substrates using glancing angle deposition method. The cross section of the structures was observed by field emission scanning electron microscopy. Atomic force microscopy and X-ray diffraction patterns were used to investigate the surface morphology and crystalline degree of the samples. The grain size and surface roughness of the samples were obtained using Nova software. The results showed that the porosity percentage of the star shape thin films depended on the grain size and shape of the structures. The electrical resistance of the star shape sculptured thin films was obtained using a four-point probe technique. Finally, electrical resistance dependence on the porosity percentage was investigated.

Keywords: Sculptured thin film, Star shape, Glancing angle deposition, Porosity, Resistance, Tunneling effect.

[*] ***Corresponding author:*** *Fatemeh Abdi, Department of Engineering Sciences, Faculty of Advanced Technologies, University of Mohaghegh Ardabili, Namin, Iran. Email: F.Abdi@uma.ac.ir.*

Introduction

A thin film is a layer of material that is about a few Nanometers to several micrometers thick. due to their low thickness, high surface to volume ratio, and the special physical structure of thin films (which is a direct result of their growth process), they have special properties that are very different from the properties of their bulk materials. Therefore, the properties of the thin film depend on the dimensions, geometric shape and microstructure of the films [1].

There are two chemical and physical methods for preparing thin films. In chemical methods, controlled chemical reactions are used to prepare thin films. In physical methods, however, a source of initial material is used and the particles deposited on the substrate by evaporation or bombardment of the material in vacuum conditions. It should be noted that the properties of the film are affected by the deposition method, and films prepared by different methods have different structures and properties [1]. One of the main advantages of physical depositions over chemical methods is that the films obtained from these methods have a higher degree of purity. As evaporative particles land perpendicular to the substrate, a uniformity thin layer is formed. But in the oblique angle deposition method (OAD method), the primary particles create shadow areas behind them, which are protected from the landing of other particles, and as a result, not much growth takes place in these shadow areas [2, 3]. In OAD method, the primary clusters that form on the substrate have a diameter of 3-5 nm [2 ,3]. The shadow effect causes the descending atoms to join these primary nuclei and continue to grow in these areas, creating inclined columnar structures [4-6]. The diameter of the resulting columnar structures is about 10-100 nm [2, 3].

Glancing angle deposition is a type of physical deposition in which evaporative particles land on the substrate at angles greater than 85 degrees (relative to the line perpendicular to the substrate surface). In this type of deposition, due to the shadowing effect, the obtained films are not uniform and are porous, and their main use is due to their porosity [7-8]. The amount of porosity and consequently the density of these films can be controlled by adjusting the angle of the substrate relative to the evaporation source [9]. By the glancing angle deposition method, various microstructures can be achieved by using substrate movements [10 and 11]. In order to form sculptured thin films, the temperature of the substrate must be low, because otherwise, the descending atoms will obtain the necessary energy to overcome the shadowing effect from the substrate temperature [12].

Due to the fact that in Nano scale, the properties of Nanoparticles are highly dependent on the shape and size of Nanoparticles, by controlling the shape and size of Nanoparticles, the properties of thin films can be controlled.

Manganese as a material with high electrical resistance, low thermoelectric power and high stability, is a good candidate for the electric applications. [13]. So far, much research has been done on the investigation of electrical resistance of conventional manganese thin films [14-19]. But so far, the electrical resistance of manganese sculptured thin films has not been studied. Due to the fact that the sculpted thin films are porous films, it is very attractive to study the electrical resistance of these thin films. In this work, by preparing manganese star-shaped thin films and investigating the structural properties, the dependence of the electrical resistance of the star-shaped sculpted thin layer on the dimensions and porosity of the films has been investigated.

The study of the electrical properties of thin films for use in electronic devices is of particular importance, and so far many researchers have investigated the electrical properties depending on the dimensions of the thin film theoretically [20-35] and experimentally [36-41]. In all these studies, it has been shown that the electrical resistance decreases with the increase in the thickness of the thin film, and the reason for this is attributed to the reduction of electron scattering from the surface. Considering that sculptured thin films are porous structures and the electron current mechanism in these structures is different from ordinary thin films and is based on the tunneling theory, the electrical properties dependence on the porosity and thickness of these structures have not been investigated so far. In this work, we investigated the dependence of electrical properties depending on porosity and thickness by making porous star-shaped structures.

Experimental

To begin with, the glass substrates were cut to 2 cm× 2cm and cleaned in an ultrasonic bath, first in acetone and then in alcohol. The substrates were glued to the substrate holder using vacuum adhesive. Manganese with a purity of 99.9% was considered coating material. Deposition was performed at room temperature and at an initial pressure of 2×10^{-7} mbar using the Edward coating device (Edwards E19 A3) and using the Electron beam. The deposition angle was considered to be 80 degrees with respect to the perpendicular to the substrate. To prepare star-shaped structures with different 3-fold (3N) and 4-fold (4N) symmetries, substrate rotations were used at appropriate angles during the glancing angle deposition process.

The angles and arm lengths of star-shaped structures for different symmetries are given in Table 1 and will be explained below. Substrate rotation was performed by the rotating motor connected to the substrate. Rotation speed was controlled by the computer system to which the program was written and installed. During the coating process, the temperature of the substrate was constant and the thickness of the films and the deposition rate of 1Å/s was controlled by a quartz crystal inspector (Sigma Instruments, SQM-160, USA) located near the substrate.

Table 1. Rotation of substrate to produce Mn star shape sculptured thin films with 3-fold and 4-fold symmetries.

3-fold symmetry		**4-fold symmetry**	
Length (nm)	**Rotation (degree)**	**Length (nm)**	**Rotation (degree)**
120	-	120	-
60	180	60	180
60	300	60	270
60	180	60	180
60	300	60	270
60	180	60	180
30	-	60	270
30	180	60	180
30	300	30	-
30	180	30	180
30	300	30	270
30	180	30	180
15	-	30	270
15	180	30	180
15	300	30	270
15	180	30	180
15	300	15	-
15	180	15	180
-	-	15	270
-	-	15	180
-	-	15	270
-	-	15	180
-	-	15	270
-	-	15	180

The steps of forming the star shape sculptured thin film with triple (3N) symmetry were performed as follows.

1 -The substrate was fixed in the initial position and a thin layer of 120 nm manganese was deposited.

2 -The substrate was rotated 180 degrees and a thin layer of 60 nm manganese was deposited.

3 -The substrate was rotated 180 degrees to return to the position of stage 1 and then rotated by 120 degrees and a thin layer of 60 nm manganese was deposited.

4- The substrate was rotated 180 degrees and a thin layer of 60 nm manganese was deposited.

5-The substrate was rotated 180 ° to return to the position of step 3 and then rotated 120 ° and a 60 nm thin layer of manganese was deposited.

6 -The substrate was rotated 180 degrees and a thin layer of 60 nm manganese was deposited.

7- The substrate was rotated 180 degrees to return to the position of step 5 and then rotated 120 degrees and a 30 nm thin layer of manganese was deposited.

8- The substrate was rotated 180 degrees and a thin layer of 30 nm manganese was deposited.

9-The substrate was rotated 180 degrees to return to the position of step 7 and then rotated with 120 degrees and the 30 nm thin layer of manganese was deposited.

10- The substrate was rotated 180 degrees and a 30 nm thin layer of manganese was deposited.

11 -The substrate was rotated 180 degrees to return to the position of step 9 and then rotated by 120 degrees and a 30 nm thin layer of manganese was deposited.

12- The substrate was rotated 180 degrees and a 30 nm thin layer of manganese was deposited.

13 -The substrate was rotated 180 degrees to return to the position of step 11 and then rotated with 120 degrees and the 15 nm thin layer of manganese was deposited.

14- The substrate was rotated 180 degrees and a 15 nm thin layer of manganese was deposited.

15- The substrate was rotated 180 degrees to return to the position of step 13 and then rotated with 120 degrees and the 15 nm thin layer of manganese was deposited.

16 -The substrate was rotated 180 degrees and a 15 nm thin layer of manganese was deposited.

17- The substrate was rotated 180 degrees to return to the position of step 15 and then rotated with 120 degrees and the 15 nm thin layer of manganese was deposited.

18- The substrate was rotated 180 degrees and a 15 nm thin layer of manganese was deposited.

A schematic of the triple symmetry star-shaped structures made in this work is shown in Figure 1.

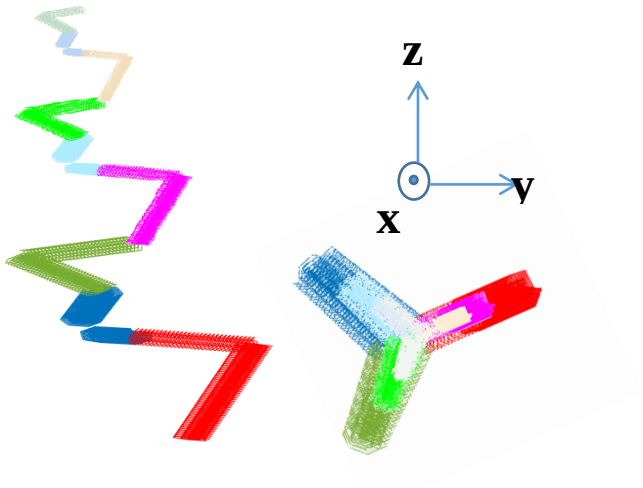

Figure 1. Schematic of Nano star with 3-fold symmetry.

Preparation of star-shaped thin films with 4-fold symmetries was done as usual, with the difference that the work steps are more than the formation steps of 3-fold star-shaped thin film and the angle of rotation was 90 degrees instead of 120 degrees.

After the formation of star-shaped thin films with different symmetries, a field emission scanning electron microscope (FESEM) (Hitachi S-4100 SEM, Japan) was used to observe them. The surface morphology of the obtained structures was examined using atomic force microscope (AFM) images (Auto Probe PC, Park Scientific Instrument, USA) and the grain size and surface porosity were obtained using Nova software. The crystalline degree of the samples was determined by studying the X-ray diffraction pattern (XRD) (CuK _ radiation; 40 kV, 30 mA). The electrical resistance of the star-shaped sculptured thin films with different symmetries was obtained using a four-point probe device and the relationship between structural properties and electrical resistance was investigated.

Results and discussions

FESEM and AFM results

Figures 2 and 3 show the FESEM images of star-shaped thin films with 3-fold and 4-fold symmetries respectively. Figure 4 show the surface of star-shaped thin films with 4-fold symmetries in large scale. It is clear from these images that the star-shaped structures with the desired symmetries were formed.

Comparison of FESEM images of star-shape structures with different symmetries shows that star-shaped structures with 4-fold symmetry (Figure 3) have large grains with more void fraction. This is due to the greater shadowing effect in this structure. In fact, in the glancing angle deposition method, the primary particles that are placed on the substrate, create shadow areas around themselves that are protected from flux landing, growth continues in the initial regions.

The porosity percentage for star-shape thin films with different symmetries was obtained using j micro vision software. The porosity percentages for structures with 3-fold and 4-fold symmetries gained 10% and 22%, respectively, and also given in the second column of Table 2. The thickness of the star-shaped thin films with different symmetries is also given in the third column of Table 2. The thickness is 400 nm and 500 nm for star-shaped structures with 3-fold and 4-fold symmetries, respectively.

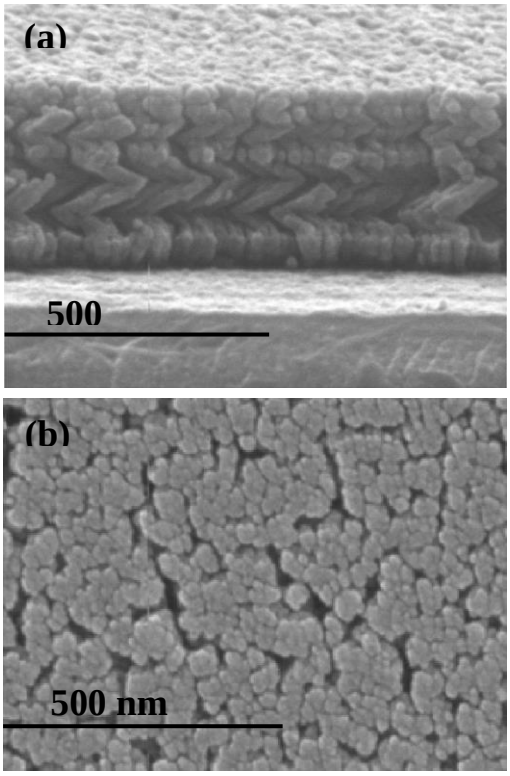

Figure 2. FESEM images of Mn Nano-star with 3-fold symmetry. (a) Cross-sectional image, (b) Surface image

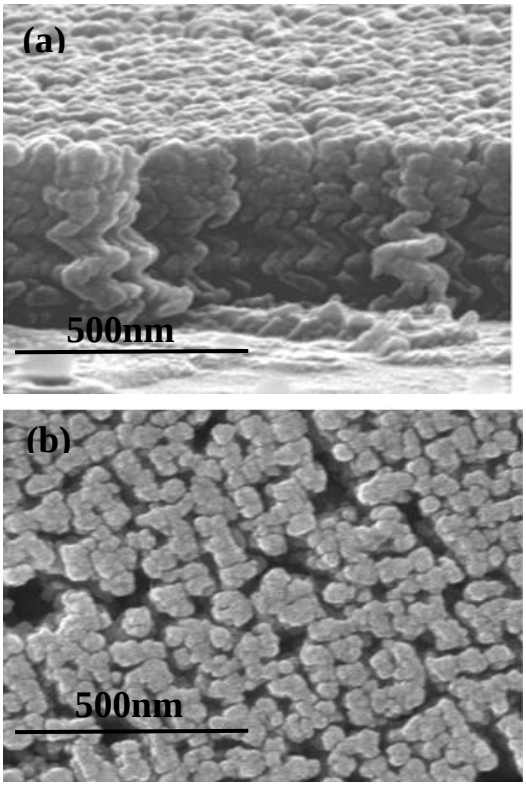

Figure 3. FESEM images of Mn Nano-star with 4-fold symmetry: (a) Cross-sectional image (b) Surface image.

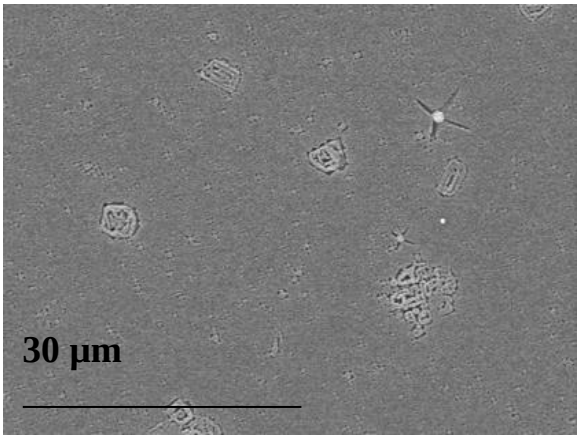

Figure 4. Surface image obtained with higher magnification of Mn Nano star with 4-fold Symmetry.

Table 2. Parameters calculated from AFM images and XRD patterns.

Sample	**3-fold**	**4-fold**
porosity	10%	22%
Thickness (nm)	400	500
Grain Size (nm)	8	32
Average Roughness (nm)	4	16
Rms (nm)	6	20.3
Crystal size (nm)	-	22

Figure 5 shows 2D and 3D AFM images of star-shaped structures with 3-fold and 4-fold symmetries. Figure 5(a) shows that star-shaped structure with 3-fold symmetry has small grains. It is also clear from Figure 5(b) that the star-shaped structure with 4-fold symmetry has large grains. Grain size, surface roughness and deviation from the mean (rms) are given in Table 2. The results show that 4-fold structures with the large grains also have more surface roughness.

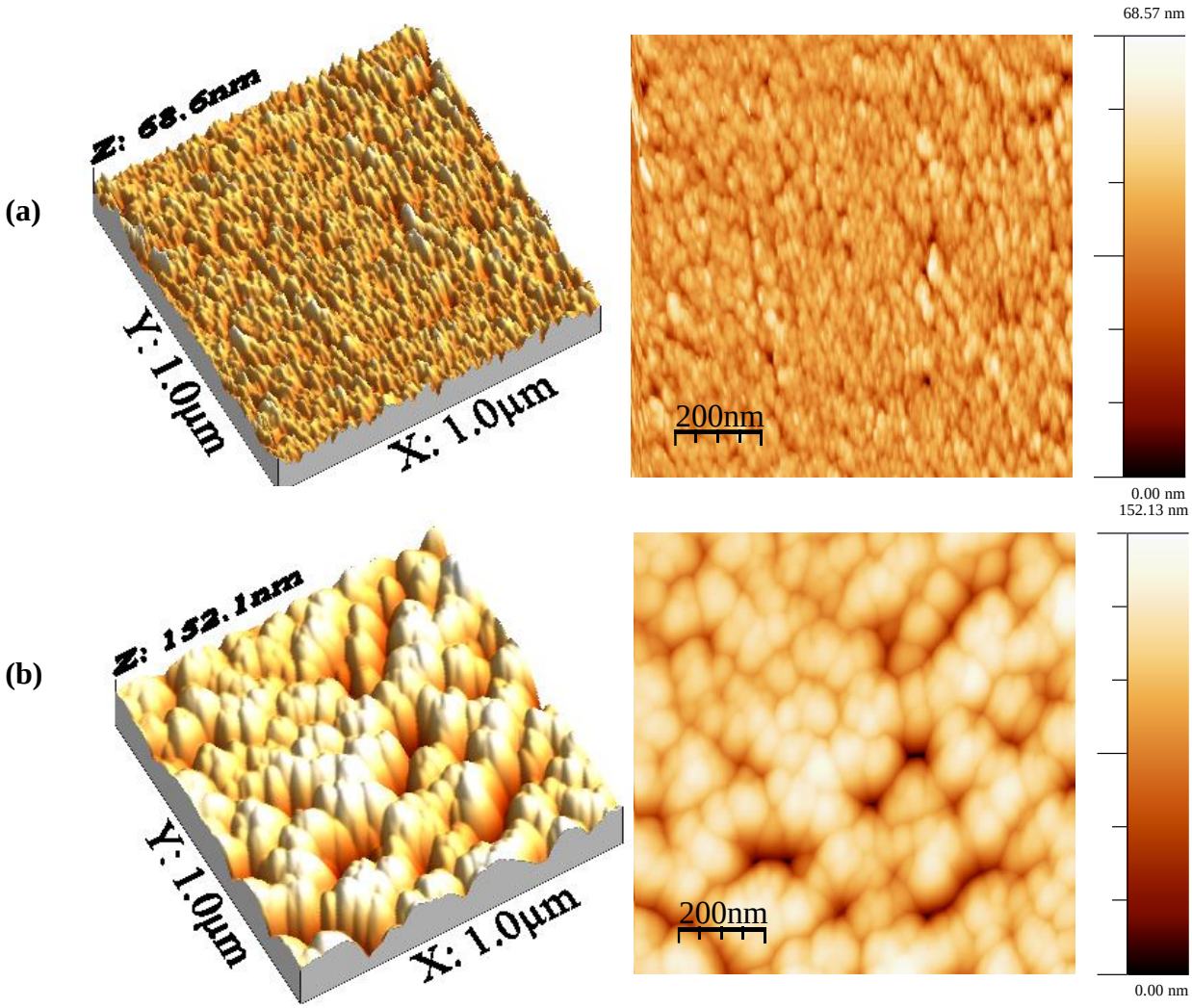

Figure 5. 2D and 3D AFM images of star shape sculptured Mn thin films. (a) 3N symmetry, (b) 4N symmetry.

Crystal structure analysis

Figure 6 (a-b) show the x-ray diffraction pattern of star-shaped thin films with 3-fold and 4-fold symmetries respectively. Figure 6 (a), which shows the diffraction pattern of a star-shaped thin film with 3-fold symmetry, shows that this structure is amorphous. Figures 6 (b) which show the diffraction pattern of star-shaped thin films with 4-fold symmetry, show that this thin films have a crystalline structure and the diffraction spectrum of these structures has a peak at a diffraction angle of 43.07 °, which is related to manganese phase of Mn(330) (according to standard card number (00-020-0180). Figure 7 (b) show that the crystalline degree of star shape structure with 4-fold symmetry is higher than the structure with 3-fold symmetry. This is due to the larger grains, better crystal growth, and larger crystal size of the star-shaped structure with 4-fold symmetry. The crystal size, calculated using the Debbie-Scherr equation, is given in the seventh column of Table 2.

$$(W0^2 - W_i^2)^{1/2} = \frac{k\lambda}{D\cos\theta} \quad (1)$$

In the above relation, D is the size of the crystal, θ is the diffraction angle, λ is the X-ray wavelength, Wi is the width at half the maximum peak, W0 is the width at the maximum half for the standard sample, and k is a constant, which is usually considered one.

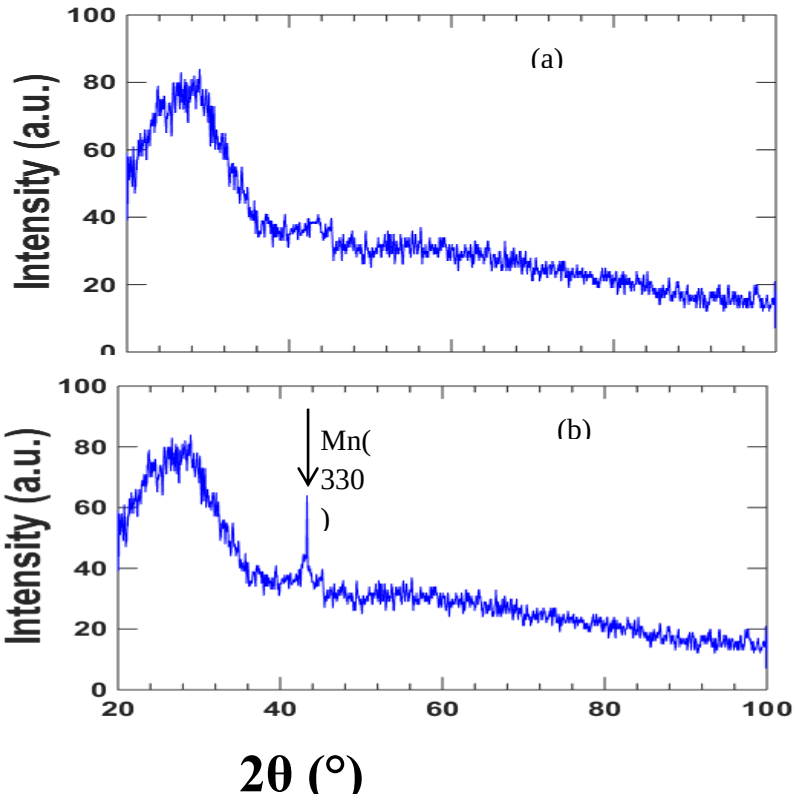

Figure 6. X-ray diffraction patterns of Mn star shap structures. (a) 3N symmetry, (b) 4N symmetry.

Electrical measurement results

Electrical measurements of the samples produced in this work were performed with a four-point probe tool. In order to investigate the effect of porosity on the electrical properties of sculptured thin films, current voltage curves (I-V) of the samples were recorded.

The electrical resistance (R) of star-shaped thin films with different symmetries were calculated using the following equation, and the results are shown in Figure 7.

$$R = \frac{\pi}{\ln 2}\left(\frac{V}{I}\right) \quad (2)$$

In this relation, t is the film thickness, V is the measured voltage and I is the current applied to the film. The results show that the electrical resistance of the star-shaped thin film with 4-fold symmetry is higher than the other sample. The reason is the greater porosity percentage of this structure compared to the other. On the other word Because the basis of current (electron motion) in

sculptural thin films is the tunneling effect and the tunneling effect decreases with increasing porosity percentage, so star-shaped structure with 4-fold symmetry has the lowest current and the highest electrical resistance.

In the conventional thin films, with the increase in thickness, the electrical resistance decreases due to the reduction of scattering effect from the surface, but the results of this work showed that for sculptured thin films, the resistance is dependent on the porosity. On the other word the star-shaped structures with 4-fold symmetry, although they were thicker than the star-shaped layers with 3-fold symmetry, but they have greater electrical resistance due to greater porosity

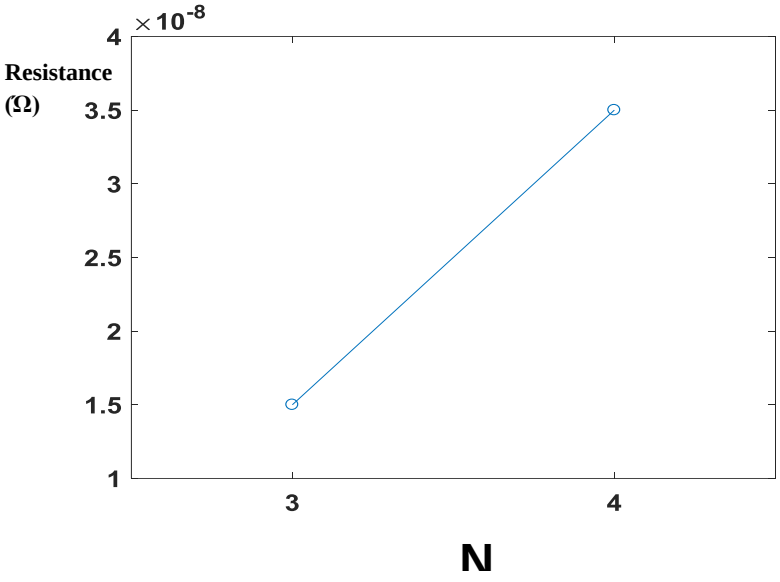

Figure 7. Resistance of the structures with 3N, 4N and 5N symmetries.

Conclusions

Manganese star-shaped thin films with different 3-fold and 4-fold symmetries were made on the glass substrate. The surface morphology of the samples and the crystalline degree of the structures were studied using atomic force microscopy and X-ray diffraction pattern respectively. The star-shaped cross-section of the structures as well as the relative porosity of the structures were observed by field emission scanning electron microscopy. The results showed that the star-shaped thin films with 4-fold symmetry have more porosity percentage, larger grains and a better crystalline degree due to the greater shadowing effect. Measurement of electrical resistance using a four-point probe device showed that thin star-shaped thin film with 4-fold symmetry has high electrical resistance, which was attributed to the more void fraction of the structures. The results showed that the electrical resistance of sculptured thin films depends on the porosity of the structures, and with the increase in the porosity percentage, the electrical resistance increases. On the other words, for

sculptured thin films, the thin film with more porosity percentage has more electrical resistance despite its greater thickness, While in normal thin films, electrical resistance decreases with increasing thickness.

Acknowledgment

We would like to thank the university of Tehran and university of Mohaghegh Ardabili for their support.

References

1. Flory F, Escoubas L. Optical properties of nanostructured thin films. Progress in quantum electronics. 2004 Jan 1;28(2):89-112.

2. Wang F, Lakhtakia A. Response of slanted chiral sculptured thin films to dipolar sources. Optics communications. 2004 May 1;235(1-3):133-51.

3. Wang F, Lakhtakia A. Response of slanted chiral sculptured thin films to dipolar sources. Optics communications. 2004 May 1;235(1-3):133-51.

4. Nieuwenhuizen JM, Haanstra H. Microfractography of thin films. Philips Tech Rev. 1966;27(3):87-91.

5. Messier R, Yehoda JE. Geometry of thin-film morphology. Journal of applied physics. 1985 Nov 15;58(10):3739-46.

6. Motohiro T, Taga Y. Thin film retardation plate by oblique deposition. Applied optics. 1989 Jul 1;28(13):2466-82.

7. Messier R, Lakhtakia A. Sculptured thin films—II. Experiments and applications. Materials Research Innovations. 1999 Jan 1;2(4):217-22.

8. Hodgkinson I, Wu QH. Inorganic chiral optical materials. Advanced materials. 2001 Jul;13(12-13):889-97.

9. Lakhtakia A, Geddes JB. Thin-film metamaterials called sculptured thin films. Trends in Nanophysics: Theory, Experiment and Technology. 2010:59-71.

10 Lakhtakia A, Messier R. Sculptured thin films—I. Concepts. Materials Research Innovations. 1997 Dec 1;1(3):145-8.

11. Messier R, Venugopal VC, Sunal PD. Origin and evolution of sculptured thin films. Journal of Vacuum Science & Technology A: Vacuum, Surfaces, and Films. 2000 Jul 1;18(4):1538-45.

12. Suzuki MS, Taga YT. Integrated sculptured thin films. Japanese Journal of Applied Physics. 2001 Apr 1;40(4A):L358.

13. Angadi MA. Some transport properties of transition metal films. Journal of materials science. 1985 Mar;20:761-96.

14. Angadi MA, Shivaprasad SM. A new material for the fabrication of thin film resistors. Journal of materials science letters. 1984 Aug;3(8):739-42.

15. Perinati A, Piacentini GF. Thermoelectric power, Hall coefficient, and structure properties of Ta thin films rf sputtered in Ar–N2–O2. Journal of Vacuum Science and Technology. 1977 Jan;14(1):169-73.

16. Shivaprasad SM, Angadi MA. The effect of deposition rate on the electrical resistivity of thin manganese films. Journal of Physics D: Applied Physics. 1980 Aug 14;13(8):L157.

17. Shivaprasad SM, Angadi MA, Udachan LA. Temperature coefficient of resistance of thin manganese films. Thin Solid Films. 1980 Aug 15;71(1):L1-4.

18. Shivaprasad SM, Angadi MA. The effect of substrate temperature on the electrical resistivity of thin manganese films. Journal of Physics D: Applied Physics. 1981 Jun 14;14(6):1125.

19. Ammar AH. Electrical transport properties of manganese thin films. Physica B: Condensed Matter. 1996 Jul 1;225(1-2):132-6.

20. Trivedi N, Ashcroft NW. Quantum size effects in transport properties of metallic films. Physical Review B. 1988 Dec 15;38(17):12298.

21. Sondheimer EH. The mean free path of electrons in metals. Advances in physics. 2001 Sep 1;50(6):499-537.

22. Namba Y. Resistivity and temperature coefficient of thin metal films with rough surface. Japanese Journal of Applied Physics. 1970 Nov 1;9(11):1326.

23. Cottey AA. The electrical conductivity of thin metal films with very smooth surfaces. Thin Solid Films. 1968 Jan 1;1(4):297-307.

24. Tellier CR, Tosser AJ. Adequate use of the Cottey Model for the description of conduction in polycrystalline films. Active and Passive Electronic Components. 1979 Jan 1;6:37-8.

25. Liu HD, Zhao YP, Ramanath G, Murarka SP, Wang GC. Thickness dependent electrical resistivity of ultrathin (< 40 nm) Cu films. Thin Solid Films. 2001 Mar 1;384(1):151-6.

26. Rossnagel SM, Kuan TS. Alteration of Cu conductivity in the size effect regime. Journal of Vacuum Science & Technology B: Microelectronics and Nanometer Structures Processing, Measurement, and Phenomena. 2004 Jan 1;22(1):240-7.

27. Dayal D, Rudolf P, Wiβmann P. Thickness dependence of the electrical resistivity of epitaxially grown silver films. Thin Solid Films. 1981 May 15;79(2):193-9.

28. Camacho JM, Oliva AI. Morphology and electrical resistivity of metallic nanostructures. Microelectronics Journal. 2005 Mar 1;36(3-6):555-8.

29. Mayadas AF, Shatzkes M. Electrical-resistivity model for polycrystalline films: the case of arbitrary reflection at external surfaces. Physical review B. 1970 Feb 15;1(4):1382.
30. Sambles JR. The resistivity of thin metal films—some critical remarks. Thin Solid Films. 1983 Aug 26;106(4):321-31.
31. Durkan C, Welland ME. Size effects in the electrical resistivity of polycrystalline nanowires. Physical review B. 2000 May 15;61(20):14215.
32. Feder J, Rudolf P, Wissmann P. The resistivity of single-crystal copper films. Thin Solid Films. 1976 Jul 15;36(1):183-6.
33. Yarimbiyik AE, Schafft HA, Allen RA, Zaghloul ME, Blackburn DL. Modeling and simulation of resistivity of nanometer scale copper. Microelectronics Reliability. 2006 Jul 1;46(7):1050-7.
34. Fan P, Yi K, Shao JD, Fan ZX. Electrical transport in metallic films. Journal of applied physics. 2004 Mar 1;95(5):2527-31.
35. Lacy F.Developing a theoretical relationship between electrical resistivity, temperature and film thickness for conductors. Nanoscale research letters. 2011 Dec;6:1-4.
36. Brousseau JL, Bourque H, Tessier A, Leblanc RM. Electrical properties and topography of SnO2 thin films prepared by reactive sputtering. Applied surface science. 1997 Mar 1;108(3):351-8.
37. Sakashita Y, Segawa H, Tominaga K, Okada M. Dependence of electrical properties on film thickness in Pb (Zr x Ti1− x) O3 thin films produced by metalorganic chemical vapor deposition. Journal of applied physics. 1993 Jun 1;73(11):7857-63.
38. Das VD, Ganesan PG. Thickness and temperature dependence of electrical properties of semiconducting (Bi0. 75Sb0. 25) 2Te3 thin films. Solid state communications. 1998 May 1;106(5):315-20.
39. Romanov RI, Kozodaev MG, Chernikova AG, Zabrosaev IV, Chouprik AA, Zarubin SS, Novikov SM, Volkov VS, Markeev AM. Thickness-Dependent Structural and Electrical Properties of WS2 Nanosheets Obtained via the ALD-Grown WO3 Sulfurization Technique as a Channel Material for Field-Effect Transistors. ACS omega. 2021 Dec 9;6(50):34429-37.
40. He J, Li F, Chen X, Qian S, Geng W, Bi K, Mu J, Hou X, Chou X. Thickness dependence of ferroelectric and optical properties in Pb (Zr0. 53Ti0. 47) O3 thin films. Sensors. 2019 Sep 20;19(19):4073.
41. Yao JK, Ye F, Fan P. Temperature-dependent optical and electrical properties of InGaZnON thin films. Optical Materials Express. 2019 Sep 1;9(9):3781-8.
42. Domtau DL, Simiyu J, Ayieta EO, Muthoka B, Mwabora JM. Optical and electrical properties dependence on thickness of screen-printed TiO2 thin films. Journal of Materials Physics and Chemistry. 2016; 4(1),:1-3.